

1 **Thermally driven escape from Pluto's atmosphere: A**
2 **combined fluid/kinetic model**

3
4 O. J. Tucker*, J. T. Erwin, J. I. Deighan, A. N. Volkov, R. E.
5 Johnson

6 Engineering Physics, 395 McCormick Road, University of
7 Virginia, Charlottesville, Va, 22904 USA

8 Email Addresses: ojt9j@virginia.edu*, jte2c@virginia.edu,
9 jid7v@virginia.edu, av4h@virginia.edu, rej@virginia.edu

10 Phone Number: 1-434-924-3244

11

12 **Abstract:** A combined fluid/kinetic model is developed to
13 calculate thermally driven escape of N₂ from Pluto's atmosphere
14 for two solar heating conditions: no heating above 1450 km and
15 solar minimum heating conditions. In the combined model, one-
16 dimensional fluid equations are applied for the dense part of the
17 atmosphere, while the exobase region is described by a kinetic
18 model and calculated by the direct simulation Monte Carlo
19 method. Fluid and kinetic parts of the model are iteratively solved
20 in order to maintain constant total mass and energy fluxes through
21 the simulation region. Although the atmosphere was found to be
22 highly extended, with an exobase altitude at ~6000 km at solar
23 minimum, the outflow remained subsonic and the escape rate was
24 within a factor of two of the Jeans rate for the exobase
25 temperatures determined. This picture is drastically different from
26 recent predictions obtained solely using a fluid model which, in
27 itself, requires assumptions about atmospheric density, flow
28 velocity and energy flux carried away by escaping molecules at
29 infinity. Gas temperature, density, velocity and heat flux versus
30 radial distance are consistent between the hydrodynamic and
31 kinetic model up to the exobase, only when the energy flux across
32 the lower boundary and escape rate used to solve the
33 hydrodynamic equations is obtained from the kinetic model. This
34 limits the applicability of fluid models to atmospheric escape

35 problems. Finally, the recent discovery of CO at high altitudes, the
36 effect of Charon and the conditions at the New Horizon encounter
37 are briefly considered.

38 **Keywords:** Pluto; Atmospheres, Dynamics; Atmospheres,
39 Structure; Aeronomy

40

41 **1 INTRODUCTION**

42 Our understanding of Pluto's N₂ dominated atmosphere is
43 largely based on rare occultation observations in 1988 (pre-
44 perihelion), 2002 and 2006 (post-perihelion) (Elliot et al., 2007;
45 Young et al., 2008). Each observation determined the surface
46 pressure to be between 6.5-24 μbars with a peak atmospheric
47 temperature of ~100 K at a radial distance ~1250 km. At this
48 temperature and due to Pluto's low gravitational energy, e.g. 0.007
49 eV/amu at 1250 km, escape can result in significant atmospheric
50 loss. Therefore, many studies of Pluto's evolution have been aimed
51 at understanding the loss rate over time (Hubbard et al., 1990;
52 Hunten and Watson, 1982; Strobel, 2008a; Tian and Toon, 2005;
53 Trafton, 1980).

54 Using results from the occultation observations and
55 calculations of solar heating rates in continuum models of the
56 upper atmosphere, a series of authors calculated thermal escape
57 rates from Pluto's atmosphere by considering a process referred to
58 as slow hydrodynamic escape (SHE, e.g., McNutt, 1989;
59 Krasnopolsky, 1999; Strobel, 2008a). The SHE model of the
60 atmosphere is based on the premise that thermal energy of
61 molecules is efficiently converted into bulk flow energy. This
62 assumption can lead to an over-estimate of the escape rate
63 (Johnson, 2010; Volkov et al., 2011a, b) when applied to the

64 rarefied region of the atmosphere where the collisions are too
65 infrequent to maintain local thermal equilibrium. Using a
66 combined fluid/kinetic model to directly account for the non-
67 equilibrium nature of the gas flow in the upper atmosphere,
68 thermally driven escape from Pluto's atmosphere is found to occur
69 on a molecule by molecule basis resulting in an enhanced Jeans
70 escape rate (Tucker et al., 2011).

71 Globally averaged escape rates typically have been
72 estimated using fluid (Strobel, 2008a, b) or kinetic models (Tucker
73 and Johnson, 2009; Volkov et al., 2011a, b). Kinetic models can in
74 principle be applied to the entire atmosphere, but they are
75 computationally expensive when applied to a dense region of the
76 atmosphere. In the dense region of the atmosphere where collisions
77 are frequent the flow can be treated as a continuum and the use of a
78 fluid model is most efficient. In the fluid models the hydrodynamic
79 equations are solved to obtain the mass flow rate through the
80 atmosphere but are unable to account for relatively infrequent
81 collisions of upwardly moving molecules or returning molecules
82 that regulate escape in the upper atmosphere. Therefore, they
83 cannot correctly calculate the amount of heat transported through
84 the atmosphere. A combined fluid/kinetic model applied to dense
85 and rarefied parts of the atmosphere respectively avoids these

86 difficulties and provides a computationally-efficient tool for
87 simulation of the atmosphere (e.g. Marconi et al., 1996).

88 The aim of the present paper is to obtain the globally
89 averaged escape rate, gas density, temperature, velocity, and the
90 heat flux in Pluto’s atmosphere in the region between 1450 km –
91 30000 km using a combined fluid/kinetic model. We numerically
92 solve the one-dimensional (1D) hydrodynamic equations coupled
93 to a molecular kinetic model for the rarefied region of the
94 atmosphere similar to the approach used in Marconi et al. (1996).
95 Preliminary results were given in Tucker et al. (2011). Here
96 simulations are performed for no heating and solar minimum
97 heating conditions. The interaction of Pluto’s extended atmosphere
98 with Charon and the implications of the recently discovered CO
99 detection in Pluto’s extended atmosphere (Greaves et al., 2011) are
100 briefly considered. The results presented here also suggest that the
101 application of the hydrodynamic models to escape from other
102 planetary atmospheres (e.g., Murray-Clay et al., 2009; Tian, 2009;
103 Strobel, 2008a, b) can give incorrect estimates of the macroscopic
104 properties and the escape flux.

105 **2 Jeans, Hydrodynamic, and Slow Hydrodynamic Escape**

106 Although escape driven by solar heating is by its nature a
107 three-dimensional (3D) process, for comparison with previous
108 models, the thermal escape problem is formulated here by

109 considering a 1D, globally averaged, steady-state model of the
110 atmosphere, where the gas properties are functions of the radial
111 distance r , from the planet center. In this section, the applicability
112 of the fluid model to thermal escape is briefly analyzed. Based on
113 this analysis, a combined fluid/kinetic model is introduced in the
114 next section.

115 The Jeans parameter, $\lambda(r)$, the ratio of the gravitational
116 energy of a molecule $\Phi_g = GM_p m/r$ to its thermal energy kT , is
117 often used to characterize the atmospheric escape rate: i.e., $\lambda(r) =$
118 Φ_g / kT , with G the gravitational constant, M_p the planet mass, m
119 the molecular mass, k the Boltzmann constant and T the
120 temperature at r . In order to escape a planet's gravity a molecule
121 must be directed outward from the planet, have a velocity larger
122 than $v_{\text{esc}} = \sqrt{2GM_p/r}$ and have a low probability of colliding with
123 other molecules along its trajectory. The density of planetary
124 atmospheres decreases exponentially with altitude and the most
125 rarefied region is referred to as the exosphere. In this region
126 intermolecular collisions are rare, therefore the Jeans parameter is
127 typically evaluated at the lower boundary of the exosphere which
128 is referred to as the exobase r_x . Throughout the paper the subscript
129 "x" will be used to denote the values of all parameters evaluated at
130 $r = r_x$.

131 The degree of rarefaction of a gas is determined by the
 132 local Knudsen number, $Kn = l_c / l_a$, the ratio of the mean free path
 133 of the molecules, $l_c \sim c / (n\sigma)$, to an appropriate length scale for the
 134 gas density l_a . Here σ is the molecular cross section, n is the local
 135 number density, and the numerical coefficient c depends on the
 136 model of intermolecular collisions, e. g., for hard sphere molecules
 137 $c = 1/\sqrt{2}$ (Bird, 1994; Chapman and Cowling, 1970). The
 138 appropriate length l_a for planetary atmospheres is usually defined
 139 as the distance over which the density decreases by a factor of $1/e$
 140 and is called the atmospheric scale height $H = r / \lambda(r)$, so that $Kn =$
 141 l_c / H . When $Kn \ll 0.1$ the atmosphere is relatively dense so that
 142 molecules collide frequently. With increasing altitude collisions
 143 become less frequent and the exobase altitude is defined to occur
 144 where $Kn_x \sim 1$ or $n_x H_x \sigma \sim 1$.

145 Three regimes of escape are typically characterized using
 146 the Jeans parameter. If a planetary atmosphere has a relatively
 147 large Jeans parameter at the exobase for the dominant atmospheric
 148 species, thermal escape occurs on a molecule by molecule basis
 149 similar to evaporation, a process referred to as Jeans escape (Jeans,
 150 1916). In this approximation it is assumed the speed distribution at
 151 the exobase is Maxwellian, so that the molecular loss rate is
 152 $\varphi_J = \pi r_x^2 n_x \langle v_{th,x} \rangle (1 + \lambda_x) \exp(-\lambda_x)$, where $\langle v_{th,x} \rangle = (8kT_x / \pi m)^{1/2}$ is
 153 the mean thermal speed of molecules at the exobase. The

154 concomitant cooling rate, total energy of molecules escaping the
155 atmosphere per unit time, is $\langle E\phi \rangle_J = (kT_x)(2 + 1/(1 + \lambda_x))\phi_J$.
156 Modified Jeans escape rates, accounting for the non-zero gas
157 velocity at the exobase, have also been proposed (e. g.
158 Chamberlain, 1961; Yelle, 2004; Volkov et al., 2011a, b).

159 At small Jeans parameters the thermal energy of molecules
160 is comparable to or larger than the gravitational binding energy of
161 the planet at the exobase, so the bulk atmosphere can escape as a
162 hydrodynamic outflow (e.g., Öpik, 1963; Hunten, 1973; Volkov et
163 al., 2011a; Gruzinov, 2011). This is often referred to as blow off
164 resulting in escape rates much larger than the Jeans rate. Blow off
165 has been suggested to occur when $\lambda_x < \sim 2$ at the exobase altitude or
166 below (Hunten, 1973; Watson et al., 1981).

167 The slow hydrodynamic escape (SHE) model, considered
168 intermediate to Jeans and hydrodynamic escape regimes, has been
169 suggested to be applicable to a dense tightly bound atmosphere for
170 which the Jeans parameter, $\lambda(r_0)$ is larger than 10, estimated at a
171 radial distance, r_0 , considered to be in approximate thermal and
172 radiative equilibrium (e.g., Parker, 1964b; Watson et al., 1981).
173 The flow is referred to as slow because near r_0 the gravitational
174 energy Φ_g dominates the thermal energy ($C_p T$), which also
175 dominates the flow energy ($1/2 mu^2$) where C_p is the heat capacity
176 per molecule and $u(r)$ is the flow speed. However the flow

177 eventually reaches supersonic speeds above the exobase resulting
 178 in escape rates much larger than the Jeans rates. Below we provide
 179 a more detailed discussion on the application of hydrodynamic
 180 models to the slow hydrodynamic escape regime.

181 In the 1D steady-state hydrodynamic model the continuity
 182 equation leads to a constant molecular flow, given here as a flow
 183 rate, ϕ , vs. radial distance:

$$184 \quad \phi = 4\pi r^2 n(r)u(r) = 4\pi r_0^2 n(r_0)u(r_0). \quad (1a)$$

185 The radial momentum equation, in which the viscous term is
 186 dropped, is:

$$187 \quad dp/dr = n(d\Phi_g/dr - d(\frac{1}{2}mu^2)/dr) \quad (1b)$$

188 with the gas pressure $p = nkT$. Finally, the corresponding energy
 189 equation is:

$$190 \quad \frac{d}{dr} \left\{ \phi \left(\frac{1}{2} mu^2 + C_p T - \Phi_g \right) - 4\pi r^2 \kappa(T) \frac{dT}{dr} \right\} = 4\pi r^2 Q(r) \quad (1c)$$

191 where $\kappa(T)$, is the thermal conductivity, C_p is the heat capacity per
 192 molecule and $Q(r)$ accounts for the solar heating and IR cooling
 193 rates. Knowing the number density, n_0 , and temperature, T_0 , at the
 194 lower boundary, i.e. $n(r_0) = n_0$, $T(r_0) = T_0$, Eq. 1b and 1c are solved.
 195 A unique solution requires two additional parameters at the lower
 196 boundary, u_0 (or ϕ) and $(dT/dr)_0$. Unfortunately, in order to find u_0
 197 and $(dT/dr)_0$, one needs to impose assumptions about the solution
 198 behavior at $r \rightarrow \infty$.

199 Parker (1958) used the hydrodynamic equations to model
200 the thermal expansion of the solar wind in the vicinity of $\lambda(r_0) \sim 2$.
201 He subsequently extended that model to describe the expansion of
202 a stellar wind from a star with a tightly bound corona with $\lambda(r_0) >$
203 ~ 10 for which no or very little heat is deposited above r_0 (Parker
204 1964a, b). In this formulation, escape is powered by the heat flow
205 from below r_0 and the conditions imposed are $T, n \rightarrow 0$ as $r \rightarrow \infty$. It
206 was then shown that the dense atmosphere must expand according
207 to a critical solution, where the flow velocity, u , gradually
208 increases above the isothermal speed of sound. Purely subsonic
209 solutions were not permitted because they resulted in a finite
210 pressure at infinity.

211 Chamberlain (1961) re-considered the expansion of the
212 solar wind for subsonic velocities with the condition $T \rightarrow 0$ as
213 $r \rightarrow \infty$. He deemed this approach to be a slow hydrodynamic
214 expansion of the solar wind, and showed it is possible to obtain a
215 subsonic solution with the hydrodynamic equations if the energy
216 flux at infinity is 0. In this formulation the number density n
217 approaches a constant as $r \rightarrow \infty$. Later, Parker (1964b)
218 acknowledged this result as a limiting case to supersonic
219 expansion. He determined that this approximation would only
220 occur in the limit that the density at the lower boundary, n_0 , goes to
221 infinity. He showed for sufficiently large densities at r_0 , the energy

222 flux carried to infinity is non-zero for the condition $T \rightarrow 0$ and,
223 hence, the expansion can proceed supersonically. This is the
224 typical approach used in applying the SHE model to planetary
225 atmospheres (e.g., Krasnopolsky, 1999; Strobel, 2008a, b; Watson
226 et. al., 1981). Since the flow is slow, the standard procedure is to
227 integrate Eq. 1b and 1c neglecting the u^2 terms (Parker, 1964b).
228 Therefore, although $\phi \neq 0$ in Eq. 1a, u^2 is set equal to 0 in Eq. 1b
229 and 1c below an upper boundary where $1/2mu^2 \ll C_pT$, and T and n
230 are only regarded as valid out to an r where the u is a small
231 fraction of the local sound speed (McNutt, 1989; Krasnopolsky,
232 1999; Strobel, 2008a, b).

233 The SHE model has been subsequently applied to the
234 thermal expansion of planetary atmospheres in which solar EUV
235 and UV heating powers escape above r_0 (Watson et. al., 1981).
236 Particular emphasis has been placed on Pluto's atmosphere which
237 is widely thought to be escaping hydro-dynamically (e.g., McNutt,
238 1989; Krasnopolsky, 1999; Strobel, 2008a; Tian and Toon, 2005).
239 For example McNutt (1989) solved the hydrodynamic equations
240 neglecting the term C_pT in Eq. 1c to obtain an analytical solution
241 for n , T , and the escape rate ϕ , assuming the solar heating occurred
242 in a narrow region of the atmosphere. Krasnopolsky (1999)
243 retained the C_pT term, using numerical methods to solve the
244 hydrodynamic equations.

245 More recently Strobel (2008a, b) applied the SHE model to
246 the atmospheres of Titan and Pluto using more realistic lower
247 boundary conditions at a radial distance where the atmosphere is in
248 approximate radiative equilibrium. He iteratively solved Eq. 1b
249 and 1c using assumed values of φ and $(dT/dr)_0$, to find a solution
250 with the right asymptotic behavior and zero total energy flux at
251 $r \rightarrow \infty$ for Pluto (Strobel, 2008a) and matched to available density
252 data for Titan (Strobel, 2008b). Calculated N_2 escape rates from
253 Pluto, $\varphi \sim 9.4 \times 10^{26} \text{ s}^{-1}$, and Titan, $\varphi \sim 1.5 \times 10^{27} \text{ s}^{-1}$, were several
254 orders of magnitude larger than the Jeans escape rates calculated
255 using the corresponding SHE model exobase densities and
256 temperatures. For example, the most recent SHE model estimate
257 for escape from Pluto's atmosphere is $\sim 10^3$ times the Jeans rate for
258 the suggested atmospheric structure at solar minimum conditions
259 (Strobel, 2008a).

260 Tucker and Johnson (2009) tested the results for Titan
261 using a kinetic approach and did not obtain large escape rates. In
262 fact, when the temperature in Titan's upper atmosphere was
263 artificially increased so that $\lambda_x \sim 11$, similar to that at Pluto, the
264 escape rate obtained was enhanced over the Jeans rate but only by
265 a factor of ~ 1.5 . Using a kinetic model, Volkov et al. (2011a, b)
266 showed that thermal escape rate from both monatomic and
267 diatomic atmospheres, for which most of the heating occurs below

268 r_0 , differs from the Jeans rate by less than a factor of 2 if $\lambda(r_0) > \sim 6$.
269 Such a drastic difference between fluid and kinetic simulations in
270 the domain of the slow hydrodynamic escape, $\lambda(r_0) > \sim 10$, is due to
271 the incorrect treatment of the rarefied region of the atmosphere in
272 the hydrodynamic approximation.

273 The discrepancy between results obtained from solving the
274 hydrodynamic equations and kinetic simulations can be resolved
275 by using a combined fluid and kinetic approach (e.g., Marconi et
276 al., 1996). A stand-alone kinetic simulation is computationally
277 infeasible at $Kn(r_0) \sim 10^{-6}$ characteristic of the density at the lower
278 boundary typically used in modeling escape from Pluto's
279 atmosphere. Therefore, a computationally efficient model can be
280 constructed by coupling the hydrodynamic equations for the dense
281 atmosphere with kinetic simulations for the exosphere region.

282 **3 Combined Fluid/Kinetic Model of Thermal Escape**

283 A fluid/kinetic model is applied from a lower boundary r_0
284 in the atmosphere, considered to be in approximate local
285 thermodynamic equilibrium, to a top boundary r_1 where the
286 atmospheric flow is essentially free of collisions. We divide the
287 atmosphere into two regions, a fluid region where the
288 hydrodynamic equations are applicable from r_0 where $Kn \ll 1$ to
289 an intermediate boundary r_{od} chosen to correspond to $Kn \sim 0.1$, and
290 a kinetic region where kinetic simulations are performed by means

291 of the direct simulation Monte Carlo (DSMC) method (Bird,
 292 1994), from r_{od} to r_1 where $Kn \gg 1$.

293 When solving the fluid equations we make no assumptions
 294 about the n and T at infinity. Consistent with the SHE model we
 295 drop the $u(r)^2$ terms. It is possible to include such terms in both the
 296 SHE and fluid/kinetic approaches. However, for a dense
 297 gravitationally bound atmosphere $u(r)^2$ can be safely neglected
 298 below the exobase (Parker, 1964b). The lower boundary conditions
 299 in the fluid region are n_0 and T_0 , while the parameters φ and $\langle E\varphi \rangle_{r_0}$,
 300 the particle and energy flow across r_0 , in Eq. 2b are determined by
 301 the DSMC part of the model. The pressure and the heat flow, given
 302 by Eq. (2a, b), are determined from the integration of Eq. 1b and
 303 1c using the total heating rate $\beta(r) = r_0^{-2} [\int_{r_0}^{\infty} Q(r) dr]$ with $\beta \rightarrow \beta_0$
 304 as $r \rightarrow \infty$, as defined in Strobel (2008a), and $\langle E\varphi \rangle_{r_0}$ is obtained as
 305 the constant of integration:

$$306 \quad p = p_0 \exp \left[- \int \frac{\lambda(r)}{r} dr \right] \quad (2a)$$

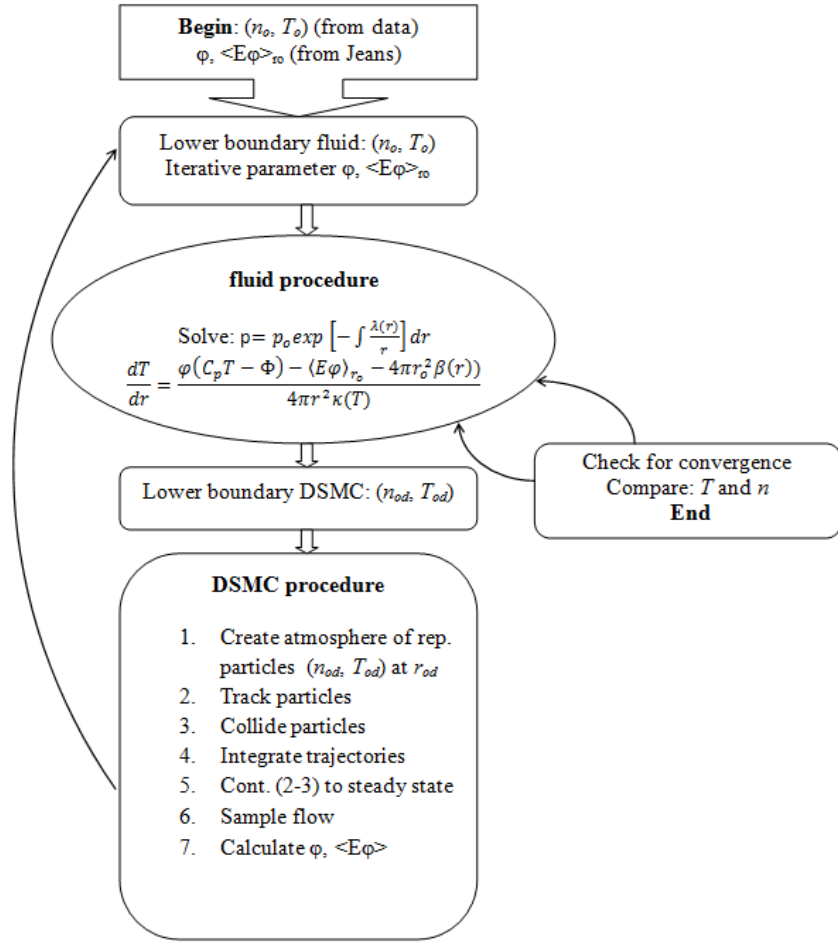
$$307 \quad \varphi(C_p T - \Phi_g) - 4\pi r^2 \kappa(T) \frac{dT}{dr} = \langle E\varphi \rangle_{r_0} + 4\pi r_0^2 \beta(r) \quad (2b)$$

308 Since the fluid model requires initial values for φ and $\langle E\varphi \rangle_{r_0}$, for
 309 the $\beta_0=0$ case we began by assuming an isothermal, hydrostatic
 310 atmosphere, $d(nkT_0)/dr = n [d\Phi_g/dr]$, and used a DSMC simulation
 311 for such an atmosphere starting at $Kn(r_{od}) \sim 0.1$ to obtain the

312 initial estimates. Therefore unlike the SHE model we do not
313 assume that the energy flow at infinity is zero. In a steady state
314 atmosphere energy conservation requires that the energy carried
315 off by escaping molecules is replaced by a flow of energy into the
316 lower boundary, $\langle E\phi \rangle_{r_0}$, with $\langle E\phi \rangle = \langle E\phi \rangle_{r_0} + 4\pi r_0^2 \beta_0$. With such
317 starting conditions, the fluid/kinetic model typically obtained a
318 converged solution in 4 iterations. That is, the temperatures agree
319 within $< 3\%$ and densities agree within $< 2\%$ in the region where
320 $0.1 < Kn < 1$.

321 As schematically presented in Fig. 1 we solve the Eq. (2a,
322 b) for the density and temperature up to the exobase and iteratively
323 obtain ϕ and $\langle E\phi \rangle_{r_0}$. From that solution the resulting n_{od} and T_{od} at
324 a radius r_{od} where $Kn \sim 0.1$, which is about two scale heights
325 below the nominal exobase, are used in the DSMC simulation up
326 to an altitude many scale heights above the exobase, $Kn \gg 1$. The
327 DSMC method tracks a representative sample of atmospheric
328 molecules which are under the gravitational influence of Pluto and
329 subjected to mutual collisions. At the upper boundary of the kinetic
330 domain we obtain the particle escape rate, ϕ , and the energy flow
331 through the 1D system, $\langle E\phi \rangle$. Values of $\langle E\phi \rangle$ and ϕ from the
332 upper boundary are used to update corresponding values in the
333 fluid part of the model and then used to solve Eq. (2a, b) up to
334 $Kn=1$ during the next iteration. Likewise the results from the new

335 simulation of the hydrodynamic equations provide updated n_{od} and
336 T_{od} at $Kn(r_{\text{od}}) \sim 0.1$ for the kinetic model, which are then used to
337 obtain new values of φ and $\langle E\varphi \rangle$. This procedure is repeated until
338 we reach consistent densities, temperatures and flow velocities in
339 the region where the fluid and kinetic model overlap. That is, for
340 $Kn \leq 1$ we numerically solve Eq. 2a and 2b to obtain $n(r)$ and $T(r)$.
341 The flow velocity, $u(r)$, is given by Eq. 1a for the set of escape
342 parameters φ and $\langle E\varphi \rangle$ obtained from the DSMC simulations. We
343 consider a converged solution acceptable when the temperatures
344 and densities agree within $\sim < 3\%$ in the overlap region between
345 our fluid and kinetic models where $0.1 < Kn < 1$.
346



347

348

349

350

351

352

353

354

355

356

Figure 1: Schematic of the numerical implementation of the fluid/kinetic model. To obtain solutions of the hydrodynamic equations at r_0 where $Kn < 0.1$, n_0 and T_0 are given, and ϕ and $\langle E\phi \rangle_{r_0}$ are obtained iteratively using the DSMC method. An initial guess of the energy flow into the lower boundary $\langle E\phi \rangle_{r_0}$ is used to solve Eq. 2a and 2b up to $Kn \sim 1$. From the fluid solution n_{od} and T_{od} calculated at $Kn_{od} \sim 0.1$ are used in the DSMC simulation up to $Kn \gg 0.1$ to obtain updated ϕ and $\langle E\phi \rangle_{r_0}$. The iterations are continued until temperature, density and heat flux are consistent

357 between the fluid and DSMC solutions in the overlap region of
358 $0.1 < Kn < 1$.

359

360 In the low Knudsen number regime Eq. 2a and 2b were
361 solved simultaneously using a 4th order Runge-Kutta method with
362 the adaptive radial step-size Runge-Kutta-Fehlberg method
363 (Burden and Faires, 2005), to ensure a relative tolerance of 10^{-8} for
364 $n(r)$ and $T(r)$. The integration steps were between 0.1 and 2 km
365 with the finer resolution necessary to resolve the faster change in
366 temperature near the lower boundary and the narrow heating peak.
367 The heating/ cooling models described in Strobel (2008a) are used
368 for the solar heating due to N_2 and CH_4 absorption bands
369 (including UV, EUV, and near-IR) and CO radiative cooling.
370 Since the heating and cooling rates depend on the temperature and
371 column of gas above a given radial position in the atmosphere, the
372 spatial distribution in the net heating rate is recalculated using the
373 new density profile. These iterations are performed until energy
374 conservation is achieved between $\langle E\phi \rangle_{r_0}$, β_0 , and $\langle E\phi \rangle$.

375 The DSMC method applied in the kinetic region $Kn > 0.1$
376 in effect solves the Boltzmann kinetic equation by the directly
377 modeling the stochastic nature of the molecular motion in the gas
378 flow using Monte Carlo techniques (Bird, 1994). The DSMC
379 method uses a set of modeling molecules in order to calculate the

380 gas properties of the atmosphere at a molecular level. Collisions
381 between molecules are calculated in discrete radial cells based on
382 the local values of the relative speed, cross section and density.
383 Therefore, the DSMC method is a direct approach for describing
384 the transition in an atmosphere from collisional to collisionless
385 flow. In such a model the conductive heat transfer is represented
386 microscopically.

387 At the lower boundary of the DSMC domain, r_{od} , the
388 density n_{od} and temperature T_{od} are taken from the solutions of the
389 fluid equations as discussed. Although in the DSMC simulations
390 molecular motion and collisions are tracked in 3D, in this paper,
391 Pluto's atmosphere is assumed to be spherically symmetric and so
392 the resulting properties depend only on r , consistent with previous
393 models for Pluto's atmosphere (Krasnopolsky, 1999; McNutt,
394 1989; Strobel, 2008a). Therefore, in the simulation domain when
395 evaluating the collision probabilities the molecular velocities and
396 positions are rotated to a common radial axis. When molecules
397 traverse the DSMC upper boundary, those with velocities greater
398 than the escape velocity and directed outward are assumed to
399 escape and the others are specularly reflected. The reflected
400 molecules represent molecules with trajectories that would
401 eventually return to the simulation domain.

402 In the DSMC method the time step is chosen to be much
403 smaller than the mean collision time and the cell widths in the flow
404 direction are kept much smaller than l_c and H following the general
405 recommendations in Bird (1994). We use variable cell widths in
406 the radial direction which were approximately $1/3^{\text{rd}}$ of the local
407 mean free path and capped at 10% of the local scale height for
408 mean free paths larger than the local atmospheric e-folding. A
409 time step of $\sim 1 - 2.5$ s provided energy conservation and ensured
410 that every molecule would have no more than 1 collision over a
411 time step on average. After $\sim 5 \times 10^6$ s the macroscopic properties
412 of the flow were sampled for an additional 5×10^7 s. The number
413 of representative molecules was chosen to ensure a sufficient
414 number of molecules (>200) in the upper most cell, typically we
415 used several $10^3 - 10^5$ representative molecules to describe the flow
416 in the kinetic region. The upper boundary location was increased
417 until the escape rate varied by less than 5% with increasing upper
418 boundary. Likewise, when using the converged fluid solution with
419 a DSMC lower boundary deeper in the atmosphere, i.e., choosing a
420 point from the fluid solution between $0.01 < Kn(r_{\text{od}}) < 0.1$, did not
421 significantly affect the results.

422 Collisions between atmospheric molecules were computed
423 using both the hard sphere (HS) model and the variable hard
424 sphere (VHS) model (Bird, 1994). To ensure consistency between

425 the fluid and kinetic models, we also used the Larsen-Borgnakke
426 (LB) approximation for internal energy and the VHS cross section
427 is parameterized to the temperature dependent thermal
428 conductivity $\kappa(T) = \kappa_0 T^\omega$ for the Maxwell gas, $\omega = 1$. The VHS
429 cross section, relevant for low speed molecular collisions, depends
430 on the relative collision speed v_r , $\sigma = \sigma_0(\langle v_{r0} \rangle / \langle v_r \rangle)$: where σ_0 is a
431 reference cross section determined from the thermal conductivity
432 and $\langle v_{r0} \rangle$ is the average relative velocity with both values obtained
433 for T_0 assuming the Maxwellian speed distribution. At
434 temperatures characteristic for Pluto's upper atmosphere, the N_2
435 vibrational modes are assumed not to be excited so that the LB
436 model is used only for two rotational degrees of freedom. The
437 initial internal energy for each molecule is set at the lower
438 boundary of the DSMC regime, r_{od} , based on a Maxwell-
439 Boltzmann energy distribution and neglecting changes in rotational
440 levels due to IR cooling between collisions.

441 **4 Results for Pluto's Atmosphere**

442 **Table 1: Parameters for fluid/kinetic model**

| Parameter | HS model | VHS model |
|---|------------------|--|
| heat capacity/molecule: C_p | $(3/2)k$ | $(5/2)k$ |
| viscosity exponent: ω ($\kappa(T) = \kappa_0 T^\omega$) | 1/2 | *1 |
| collision cross section: σ ($\times 10^{-15}$) cm^{-2} | $\sigma_0 = 9.0$ | $^+ \sigma = \sigma_0(\langle v_{r0} \rangle / v_r)$ |

443 Parameters for N_2 used in the fluid/kinetic. The lower boundary
444 radial distance is $r_0 = 1450$ km where $n(r_0) = 4 \times 10^{12} \text{ cm}^{-3}$ ($Kn_0 \sim 10^{-6}$), $T(r_0) = 88.2$ K. *The viscosity exponent for the VHS model and

446 $\kappa_0 = 9.37 \text{ erg cm}^{-1} \text{ s}^{-2} \text{ K}^{-2}$ are taken from Strobel (2008a). ⁺The
447 average relative velocity at r_0 is defined by $\langle v_{r,0} \rangle = (16kT_0/\pi m)^{1/2}$.

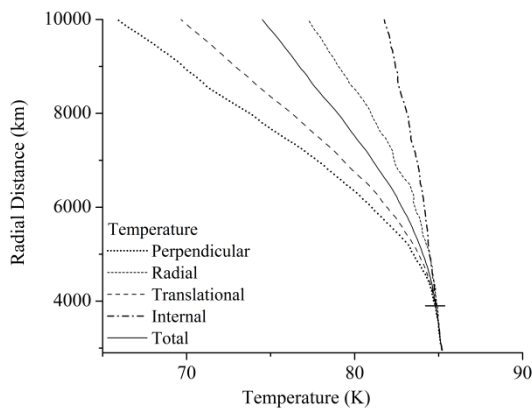
448

449 The 1D radial fluid/kinetic model is applied to a region in
450 Pluto's atmosphere from $r_0 = 1450 \text{ km}$ up to $r_1 = 30000 \text{ km}$ for $n_0 =$
451 $4 \times 10^{12} \text{ cm}^{-3}$ ($Kn_0 \sim 10^{-6}$) and $T_0 = 88.2 \text{ K}$ consistent with Strobel
452 (2008a). Pluto's orbital axis is nearly parallel to its orbital plane
453 which will result in the structure of the atmosphere being non-
454 isotropic over the globe, and the amount of solar heating is also
455 variable dependent upon the relative abundances of CH_4 and CO
456 present in the atmosphere. However, for the purpose of this study
457 we assume a globally averaged atmosphere and adopted solar
458 minimum heating rates from Strobel (2008a) to compare with the
459 SHE model results. Further studies should be done using a 3D
460 model as the amounts of CH_4 and CO in the atmosphere are better
461 constrained.

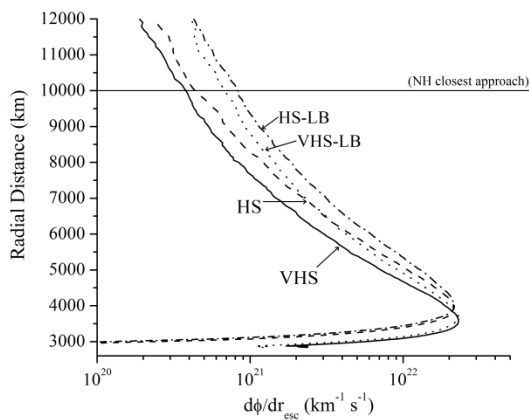
462 We first obtained a converged solution for density and
463 temperature versus radial distance with the fluid/kinetic approach
464 using the HS collision model with the DSMC simulation. To
465 compare the effects of using the HS, HS-LB, VHS and VHS-LB
466 collision models on φ , $n(r)$, $T(r)$ and $u(r)$ within the DSMC model,
467 the following lower boundary conditions were adopted from the
468 converged fluid/kinetic (HS) model $r_{\text{od}} = 2836 \text{ km}$ where $\lambda_{\text{od}} = 12$,

469 $n_{\text{od}} = 2.9 \times 10^7 \text{ cm}^3$ and $T_{\text{od}} = 85.5 \text{ K}$. Using the conductivity for
470 the Maxwell molecules at T_0 (Strobel, 2008a), we obtained a
471 reference value for the HS cross section of $\sigma_0 = 9.0 \times 10^{-15} \text{ cm}^2$, see
472 Table 1 for the model parameters. The mean free paths at the
473 lower boundary for a collision for HS and VHS molecules are $l_c =$
474 $(\sqrt{2}n\sigma_0)^{-1}$ and $l_c = (\langle v_{\text{th}} \rangle / n\sigma_0 \langle v_{r0} \rangle)$ respectively (Bird 1994), but
475 the values of l_c and $Kn(r_{\text{od}})$ for this particular case are similar: ~ 27
476 km and ~ 0.1 respectively. While the resulting density profiles did
477 not significantly depend on the choice of the collision model for
478 the parameters n_{od} and λ_{od} given above (e.g. for all results $r_x \sim$
479 3900 km), the resulting temperature profiles and escape rates were
480 slightly different: e.g., the escape rates are 4.4, 5.1, 4.3 and 4.8
481 $\times 10^{25} \text{ s}^{-1}$ for the HS, HS-LB, VHS and VHS-LB models
482 respectively. Above the exobase, as it is seen in Fig. 2a the
483 translational temperature decreases faster than the rotational
484 temperature, and the perpendicular temperature decreases faster
485 than the radial temperature. At distances increasingly above the
486 exobase the atmosphere cools approximately adiabatically as
487 collisions become increasingly infrequent.

488



489



490

491

492

Figure 2: Results of test simulation described in text $Kn(rod)=0.1$

493

and $\beta(r) = 0$ above lower boundary: exobase altitude is 3900 km

494

indicated by short horizontal curve in Fig. 2a.: (a) $T(K)$ in VHS-LB

495

model: short dashed curve perpendicular temperature, T_{perp} , dotted

496

curve radial temperature, T_r , dashed dotted curve rotational

497

temperature, T_{rot} , dashed curve translational temperature, $T_{trans} =$

498

$(T_r + 2T_{perp})/3$, solid curve total temperature, $T = (3T_{trans} + 2T_{rot})/5$.

499

(b) Production of escaping molecules, $d\phi/dr_{esc}$ ($\text{km}^{-1} \text{s}^{-1}$) vs. r : HS

500

(dashed curve), VHS (solid curve), HS-LB (dashed dotted curve),

501 VHS-LB (dotted curve). The New Horizons spacecraft distance of
 502 closest approach to Pluto will be 10000 km.

503

504 In the transition region of the atmosphere there is an
 505 altitude where it is most efficient for molecules to acquire escape
 506 trajectories. Below this altitude collisions inhibit escape and above
 507 there are too few collisions to produce escape trajectories. In the
 508 kinetic region we calculated the average number of escaping
 509 molecules produced in each radial cell, $d\phi/dr_{esc}$, by noting the
 510 altitude at which molecules that eventually traverse the top of the
 511 simulation domain, $r_1 = 30000$ km, first attained an escape velocity.
 512 Molecules that later lose their escape velocity are dropped from the

513 inventory, so the total escape rate is given by $\phi = \int_{r_0}^{r_1} (d\phi/dr)_{esc} dr$.

514 The peak in the escape rate production, Fig. 2b, occurs at the same
 515 altitude for the HS ($r \sim 4090$ km) and VHS ($r \sim 3680$ km) models
 516 with and without the internal degrees of freedom. The difference in
 517 the peak altitude is determined by the conductivity which differs
 518 between the VHS ($\kappa \propto T$) and HS models ($\kappa \propto T^{1/2}$). For the
 519 fluid/kinetic results discussed further below we used the VHS-LB
 520 model in order to have both $\kappa(T)$ and C_p consistent with the fluid
 521 model, and to allow for rotational/ translation energy exchange.

522

Table 2: SHE vs. fluid/kinetic

| | | | |
|--|------------|-----|-----|
| β_0 (10^{-3} erg cm ⁻² s ⁻¹) | No heating | 1.7 | 1.5 |
|--|------------|-----|-----|

| | SHE* | fluid/kinetic~ | SHE* | fluid/kinetic~ |
|--|-------------|--------------------|-------------|----------------|
| r_x (km) | 2700 | 3900 | 3530 | 6200 |
| n_x ($\times 10^5 \text{cm}^{-3}$) | 53 | 17 | 53 | 6.7 |
| T_x (K) [$H_x(100\text{km})$] | 48[1.2] | 85 [4.5] | 65 [2.6] | 87 [12] |
| u_x (m s^{-1}) | 1 | 5×10^{-4} | 2 | 4 |
| λ_x | 23 | 8.8 | 13 | 5.4 |
| ϕ (10^{25}s^{-1}) | 54 | 4.8 | 180 | 120 |
| ϕ/ϕ_J | $\sim 10^7$ | 1.6 | $\sim 10^3$ | 2.0 |
| $\langle E\phi \rangle / kT_0\phi$ | 0 | 1.8 | 0 | 1.8 |
| $\langle E\phi \rangle_J / kT_0\phi_J$ | ~ 1.11 | 2.02 | ~ 1.53 | 2.12 |

523

524

Exobase values for the density, temperature, bulk velocity,

525

escape rate ϕ and average energy carried off $\langle E\phi \rangle$ including the

526

corresponding values for the theoretical Jeans escape rate and

527

energy flow rate (ϕ_J , $\langle E\phi \rangle_J$) evaluated at the corresponding

528

exobase distances: simulations performed for $\beta_0=0$ and solar

529

minimum conditions for the SHE model and the fluid/kinetic

530

(VHS-LB) results shown in Fig. 3. The lower boundary radial

531

distance is $r_0 = 1450$ km where $n(r_0) = 4 \times 10^{12} \text{cm}^{-3}$ ($Kn_0 \sim 10^{-6}$),

532

$T(r_0) = 88.2$ K, $\lambda(r_0) = 23$ and $c_0 = 191$ m/s (sound speed). ~The

533

exobase altitude r_x is determined where $Kn = l_c/H = 1$,

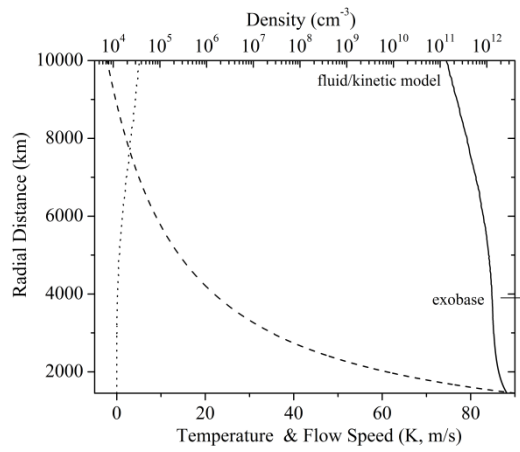
534

$l_c = \langle v_{th} \rangle / (n\sigma_0 \langle v_{r0} \rangle)$. Results are given in Table 2 from two cases

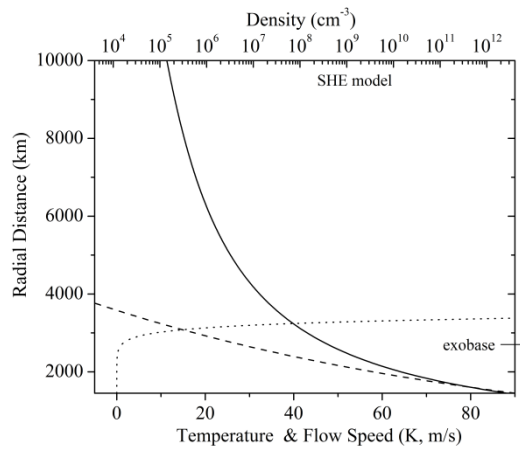
535 obtained using the combined fluid/kinetic simulation with the
 536 VHS-LB collision model. In the first case no solar heating occurs
 537 in the simulation region: i.e., $Q(r) = 0$ above r_0 so that $\beta_0=0$. Next
 538 we assume approximate solar minimum conditions where the net
 539 heating/cooling above r_0 is such that $\beta_0= 1.5 \times 10^{-3} \text{ erg cm}^{-2} \text{ s}^{-1}$
 540 which is similar to the value used in the SHE model $\beta_0= 1.7 \times 10^{-3}$
 541 $\text{erg cm}^{-2} \text{ s}^{-1}$ (Strobel, 2008a). The value of β_0 was obtained by
 542 using a fixed solar UV and EUV heating efficiency, $\varepsilon \sim 0.25$, with a
 543 cut-off in the heating at an altitude where the heat deposited was
 544 less than 1% of β_0 (Strobel, 2008a).

545 As seen in Table 2, the escape rate obtained for the $\beta_0=0$
 546 case, $4.8 \times 10^{25} \text{ s}^{-1}$, is $\sim 1.6 \times \varphi_J$, where φ_J is the Jeans rate for $T_x= 85$
 547 K and the heat flow out is $\sim 1.4 \times \langle E\varphi \rangle_J$ both evaluated at the
 548 exobase, $r_x = 3900 \text{ km}$ where $Kn = 1$. These results differ
 549 significantly from those obtained in the SHE model (e.g., $r_x = 2700$
 550 km , $n_x \sim 5.3 \times 10^6 \text{ cm}^{-3}$, $T_x = 48 \text{ K}$ and $\lambda_x \sim 23$; Strobel, 2008a)
 551 indicative of the very different atmospheric profiles as seen in Fig.
 552 3a. The change in temperature with increasing r is seen to fall off
 553 much faster in the SHE solution consistent with an overestimate in
 554 the adiabatic cooling due to the overestimate in the escape rate.
 555 Even though the SHE model has a much larger Jeans parameter at
 556 the exobase, the escape rate is an order of magnitude larger than
 557 that obtained with the fluid/kinetic model.

558



559



560

561

562

Figure 3: $n(\text{cm}^{-3})$ (top axis), $T(\text{K})$ and $u(\text{m/s})$ (bottom axis) vs.

563

radial distance: Comparison of fluid/kinetic (a) n (dashed curves),

564

T (solid curves) and u (dotted curves) to SHE model results (b) from

565

Strobel (2008a) for no heating above r_0 ($\beta_0 = 0$). The exobase

566

distance is indicated by the solid curve on right axis: 3900 km

567

fluid/kinetic model and 2700 km SHE model. The New Horizons

568

spacecraft distance of closest approach to Pluto will be 10000 km.

569

570

571

572

573

574

575

576

577

578

579

580

581

582

583

584

585

586

587

588

589

590

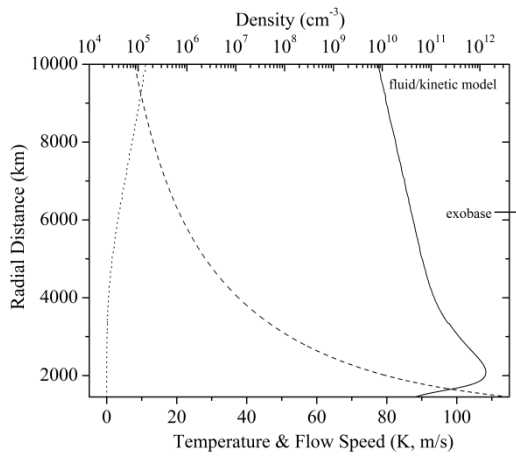
591

Numerically solving the fluid equations for $\beta_0 \neq 0$ is *very sensitive* to the choice of the input escape parameters, especially the energy carried away by escape, $\langle E\phi \rangle$. Therefore, an initial solution was achieved by incrementally adding in a small fraction of the heating rate and solving the fluid equations iteratively, but assuming Jeans escape at the exobase, $Kn=1$. Having achieved a converged solution in this manner, we used the calculated $n(r_{od})$ and $T(r_{od})$ evaluated at $Kn(r_{od}) = 0.1$ as the starting point for the first DSMC iteration. When the solar minimum heating is included the Jeans parameter at the lower boundary for the kinetic model for the converged result was $\lambda(r_{od}) \sim 9$. The SHE result taken from Strobel (2008a) is obtained by solving Eq. 1b and 1c using assumed values of ϕ and $(dT/dr)_0$, to find a solution with $n, T \rightarrow 0$ and zero total energy flux as $r \rightarrow \infty$.

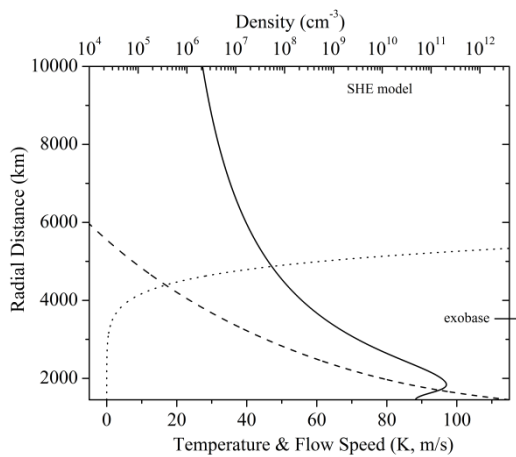
As seen in Table 2, the resulting escape rate for the solar minimum case was $1.2 \times 10^{27} \text{ s}^{-1}$ with $r_x \sim 6200 \text{ km}$, $n_x \sim 7 \times 10^5 \text{ cm}^{-3}$, $T_x \sim 87 \text{ K}$ and $\lambda_x \sim 5$. Although, the escape rate is fortuitously close to the SHE result, $1.8 \times 10^{27} \text{ s}^{-1}$, the structure of the exobase region for the SHE model is *very* different: $r_x \sim 3530 \text{ km}$, $n_x \sim 5.3 \times 10^6 \text{ cm}^{-3}$, $T_x \sim 65 \text{ K}$ and $\lambda_x \sim 13$. Therefore, although the SHE escape rate was suggested to be $>10^3 \times \phi_J$, based on the temperature and density at the exobase obtained here the escape rate is $2.0 \times \phi_J$

592 and the energy flux rate is $1.7 \times \langle E\phi \rangle_J$. The size of this
 593 enhancement to the Jeans rate is similar to that found earlier
 594 (Tucker and Johnson, 2009). Ignoring the effect on Charon, this
 595 rate is also $\sim 84\%$ of the energy-limited escape rate,
 596 $(4\pi r_0^2 \beta_0) / (\lambda_0 k T_0)$, often used in exoplanet studies (Lammer et al.,
 597 2009).

598



599



600

601

602 **Figure 4:** $n(\text{cm}^{-3})$ (top axis), $T(\text{K})$ and $u(\text{m/s})$ (bottom axis) vs.
603 radial distance: Comparison of fluid/kinetic (a) n (dashed curves),
604 T (solid curves) and u (dotted curves) to SHE model results (b) from
605 Strobel (2008a) for solar minimum heating conditions above r_0 .
606 The exobase distance is indicated by the solid curve on right axis:
607 6200 km fluid/kinetic model and 3530 km SHE model. The New
608 Horizons spacecraft distance of closest approach to Pluto will be
609 10000 km.

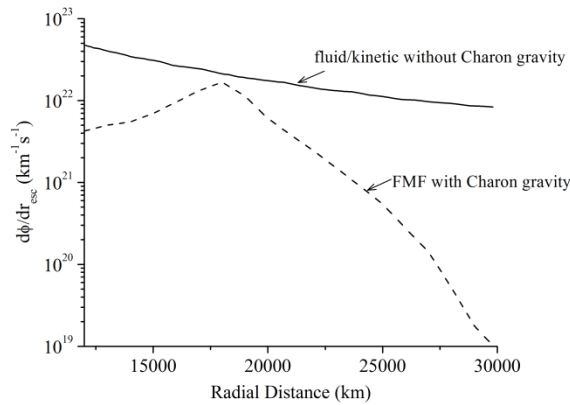
610

611 **5 Effect of Charon on Escape**

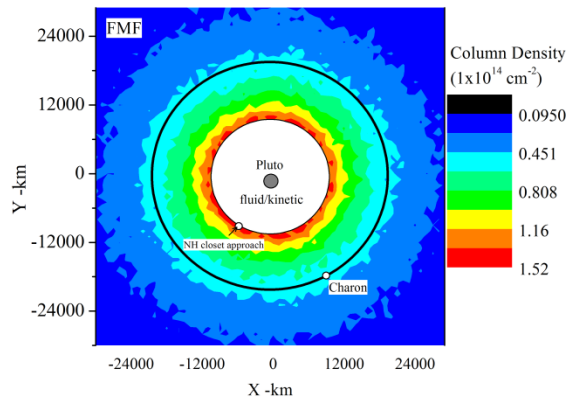
612 We examine here whether or not these results have
613 implications for Charon, which has $\frac{1}{2}$ the diameter and $\frac{1}{10}$ mass of
614 Pluto. At an orbital distance of 19500 km the Hill sphere radius
615 about Charon is at a radial distance of 12700 km from Pluto, where
616 the atmospheric density is $\sim 10^5 \text{ cm}^{-3}$ for the solar minimum case,
617 Fig. 4a. Ignoring here any tidal effect on Pluto's lower atmosphere
618 we estimated whether the effect of Charon's gravity on the
619 molecular trajectories would significantly affect the escape rate.
620 Therefore, we used the DSMC results for solar minimum
621 conditions to perform free molecular flow (FMF) simulations in
622 which molecules move under the influence of gravity from both
623 Pluto and Charon but without inter-molecular collisions. Charon is
624 assumed to have a circular orbit about Pluto and the molecular

625 trajectories are tracked in a 3D region from 10000 km to 30000 km
626 about Pluto. The FMF simulation is begun by emitting molecules
627 at $r = 10000$ km with radial velocities obtained from the
628 fluid/kinetic model for solar minimum heating conditions.
629 Escaping molecules are either emitted initially with a speed above
630 the escape speed or they gain an escape speed under the
631 gravitational influence of Charon. After several Charon orbits we
632 obtained a steady-state morphology of the gas density in the Pluto-
633 Charon system and the integrated escape rate produced versus
634 radial distance, as shown in Fig. 5(a, b).

635



636



637

638

Figure 5: (a) Production of escaping molecules $d\phi/dr_{\text{esc}}$ ($\text{km}^{-1}\text{s}^{-1}$)

639

vs. r . DSMC results for solar minimum heating conditions without

640

including Charon's gravitation influence (solid curve), as in Fig.

641

2b, compared to the fluid/kinetic result coupled to a FMF model

642

that includes Charon's gravitational effect (dashed curve). (b)

643

Contour plot of column density in the z plane Charon's northern

644

and southern hemispheres in FMF simulations including Charon's

645

gravitational influence: black curve represents Charon's orbit.

646

Particles are emitted radially with corresponding speeds according

647

to the local distribution at 10000 km. The New Horizons (NH)

648

spacecraft distance of closest approach to Pluto will be 10000 km.

649

650

For solar minimum heating conditions we estimated that

651

molecules from Pluto's atmosphere impinge upon Charon at a rate

652

of 10^{25} s^{-1} . With Charon's surface temperature of $\sim 50\text{K}$ this would

653

be equivalent to the deposition of a monolayer of molecules over 4

654 Charon orbits at $8 \times 10^{-3} \mu\text{m/yr}$. We also found that Charon has only
655 a small effect on the escape rate from Pluto's atmosphere. Charon
656 does not trap many molecules from Pluto's expanded atmosphere,
657 but rather perturbs the molecules trajectories accelerating them to
658 or decelerating them from escaping the system. The above
659 conclusions were determined by performing FMF simulations with
660 and without the gravitational influence of Charon in which we
661 found that the escape rate decreased by 3 % in simulations that
662 included Charon. This is opposite to the change in the escape rate
663 that would have occurred had we used the energy to reach the Hill
664 sphere of Charon as the escape criterion in the fluid/ kinetic
665 simulations. A contour plot of the averaged total column densities
666 over the north and south hemispheres when including Charon's
667 gravitational influence is shown in Fig. 5b. The relevance of
668 Charon is likely more significant at solar maximum heating
669 conditions and close to perihelion.

670 **6 CONCLUSIONS**

671 Hydrodynamic models have often been applied to
672 atmospheres in the solar system and to exoplanet atmospheres in
673 order to estimate escape and the concomitant adiabatic cooling of
674 the upper atmosphere (e.g., McNutt, 1989; Krasnopolsky, 1999;
675 Tian and Owen, 2005; Strobel, 2008a, b; Yelle, 2004; Tian, 2009;
676 Murray-Clay et al., 2009). Unless the Jeans parameter is < 2 well

677 below the exobase ($Kn \ll 1$), this procedure can give incorrect
678 atmospheric properties as compared to the fluid/kinetic combined
679 approach described here. The difficulties with using a continuum
680 model of thermal escape are twofold; how to, without prior
681 knowledge, define density, temperature and energy flow at infinity,
682 and how to properly define thermal conduction in the exosphere.
683 The Fourier heat flux used to solve Eq. 2b becomes invalid near
684 the exobase as discussed earlier (e.g., Johnson, 2010; Volkov et al.,
685 2011a, b). Here we use a combined fluid/kinetic model that
686 explicitly incorporates how heat conduction powers escape without
687 requiring any assumptions about the macroscopic properties of the
688 atmosphere at infinity. The hydrodynamic equations are solved
689 below the exobase, and the kinetic model is continued above where
690 the flow is essentially non-equilibrium. Such a procedure is
691 relevant not only to Pluto but to the evolution of atmospheres on
692 terrestrial bodies including recently discovered hot, rocky
693 exoplanet atmospheres.

694 For over a few decades, hydrodynamic models have been
695 used to conclude that Pluto's atmosphere is lost by a process called
696 slow hydrodynamic escape (e.g., Krasnopolsky, 1999; McNutt,
697 1989; Strobel, 2008). We reconsidered escape from Pluto using
698 the fluid/kinetic model and found that for the two cases considered,
699 thermally-driven escape occurs at a rate within a factor of two of

700 the Jeans rate for the temperature determined in the combined
701 model. That is, for a lower boundary, r_0 , in Pluto's atmosphere
702 where $\lambda(r_0) \sim 23$ and $Kn(r_0) \sim 10^{-6}$, and with all of the heat
703 deposited below r_0 (i.e., $\beta_0 = 0$), we obtain an escape rate $\phi \sim 4.8$
704 $\times 10^{25} \text{ N}_2 \text{ s}^{-1}$. For the derived exobase temperature, $T_x = 85 \text{ K}$, this is
705 ~ 1.6 times the Jeans rate ($\phi_J \sim 3.0 \times 10^{25} \text{ N}_2 \text{ s}^{-1}$) and 1.4 times the
706 Jeans energy flux ($\langle E\phi \rangle_J \sim 7.40 \times 10^{11} \text{ ergs s}^{-1}$). Furthermore we
707 find that each escaping molecule carries off an energy $\sim 2kT_0$ as
708 seen in Table 2, and not 0 as assumed in the SHE model. It is
709 interesting to note that for the same lower boundary conditions, if
710 one assumed the atmosphere was hydrostatic, the Jeans rate would
711 be $\phi_J \sim 5.6 \times 10^{25} \text{ N}_2 \text{ s}^{-1}$ and $\langle E\phi \rangle_J \sim 1.4 \times 10^{12} \text{ ergs s}^{-1}$. Therefore,
712 these simulations indicate escape is similar in nature to Jeans
713 escape, but to get the correct *exobase temperature and density*
714 needed to make a Jeans estimate, a kinetic model should be applied
715 in the non-equilibrium region of the atmosphere.

716 We also simulated Pluto's atmosphere for solar minimum
717 conditions above r_0 . For the same density and temperature at r_0 ,
718 with a similar solar minimum heating rate to that used in Strobel
719 (2008a), we obtain $\phi \sim 1.2 \times 10^{27} \text{ N}_2 \text{ s}^{-1}$. At the derived $T_x = 87 \text{ K}$
720 from the model this is ~ 2.0 times the Jeans rate ($\phi_J \sim 6.0 \times 10^{26} \text{ N}_2$
721 s^{-1}) and ~ 1.7 times the Jeans energy flux ($\langle E\phi \rangle_J \sim 1.6 \times 10^{13} \text{ ergs s}^{-1}$

722 ¹). As seen in Table 2, the escape rate for solar minimum
 723 conditions is fortuitously close to that obtained in Strobel (2008a)
 724 of $1.8 \times 10^{27} \text{ N}_2 \text{ s}^{-1}$, but the total energy flux into the lower
 725 boundary leads to a very different atmospheric structure in the
 726 exobase region. Although this energy flux is a small fraction of the
 727 energy flux added above r_0 due to solar heating,
 728 $\langle E\phi \rangle_{r_0} / (4\pi r_0^2 \beta_0) = 6.8 \times 10^{-2}$, it influences density and
 729 temperature gradients below the heating peak where $\beta(r) \rightarrow 0$ as r
 730 $\rightarrow r_0$. Furthermore the flow fields are radically different. This may
 731 be illustrated by comparing the relative magnitudes of the static, p ,
 732 and dynamic, $\frac{1}{2}mnu^2$, pressures of each model. For the radial
 733 distance examined, 1450 km – 10000 km, we find the total
 734 pressure profile of the fluid/kinetic model monotonically decreases
 735 and is dominated by the static pressure. On the other hand, the
 736 SHE model experiences a minimum in the dynamic pressure at
 737 5700 km with the region below dominated by the static pressure
 738 and the region above dominated by the dynamic pressure. The sum
 739 of the dynamic and static pressures in the SHE model also exceeds
 740 that of the fluid/kinetic model above 8200 km, suggesting that
 741 despite their similar flux rates the two models may be
 742 observationally distinguishable in their determination of Pluto's
 743 interaction with the solar wind.

744 We show here that starting at a small $Kn(r_0)$ in Pluto's
745 atmosphere, a combined fluid/kinetic model can lead to reliable
746 energy and molecule escape rates both for no heating and solar
747 minimum heating conditions in the region above 1450 km. It is
748 also clear from the fluid and DSMC results in the overlap region,
749 that for this range of Jeans parameters a fluid model *can* obtain
750 accurate temperatures densities and gas velocities with similar heat
751 fluxes up to the exobase. But this is the case *only* if the ϕ and
752 $\langle E\phi \rangle_{r_0}$ used are equal to that obtained from a kinetic simulation of
753 the exobase region. In fact, the total energy flux through the
754 system cannot be determined independently for finite $Kn(r_0)$ using
755 a fluid calculation, because it depends on the flow in the non-
756 equilibrium region of the exosphere. Numerical methods have been
757 used to solve the hydrodynamic model using a Jeans type escape
758 and energy flux at or near the exobase (Chamberlain, 1961; Yelle,
759 2004; Gruzinov, 2011). However, these models require assumed
760 values for n and T at the upper boundary.

761 We have treated Pluto's atmosphere using a single species,
762 N_2 , throughout the simulation region and have found an enhanced
763 Jeans rate like that found earlier (Tucker and Johnson, 2009).
764 Although minor species, with very different masses, will separate
765 from the N_2 profile in the region of escape (e.g., Tucker and
766 Johnson, 2009), CO should roughly track the N_2 profile described

767 here. Since the solar activity during the observations of Greaves et
768 al. (2011) in 2009/10 was close to that used for our assumed solar
769 minimum conditions, the discovery of CO at altitudes ~4500km
770 might not be surprising based on the atmospheric structure found
771 here and does not require understanding the interaction of the
772 extended atmosphere with the solar wind. Based on an assumed
773 mixing ratio of ~0.05% the CO tangential column density at 4500
774 km would be $\sim 6 \times 10^{11}$ CO cm⁻², but the temperature at this altitude
775 is 91 K as opposed to 50 K suggested by the observations.

776 Solar maximum conditions are expected to occur in 2013,
777 so that the New Horizon encounter with Pluto and Charon in 2015
778 will occur somewhere between solar maximum and minimum
779 conditions. At a distance from the sun of 33 AU and assuming the
780 same heating efficiency and cooling process, this results in $\beta_0 \sim 1.7$
781 times that used here ($\sim 2.5 \times 10^{-3}$ erg cm⁻² s⁻¹). Therefore, accurate
782 simulations of the atmospheric density at the encounter distance
783 10000 km from Pluto, and the atmospheric structure and the escape
784 rates expected during the encounter will require the use of a
785 fluid/kinetic model such as that described here. Such calculations
786 are in progress for a multispecies atmosphere.

787

788 **Acknowledgements:** We thank D. Strobel for the solar minimum
789 heating rates, L. Young for information on Pluto's atmosphere, and

790 R. Yelle and A. Gruzinov for helpful comments on atmospheric
791 escape. We also note the loss of two pioneers in the field whose
792 papers we heavily relied upon, D. Hunten and J. Elliot. This
793 research was supported by the NASA Planetary Atmospheres
794 Program and the NSF Astronomy Program.

795

References

796

Bird, G. A., 1994. Molecular Gas Dynamics and the Direct

797

Simulation of Gas Flows. Clarendon Press Oxford, New

798

York.

799

Burden, R. L. and Faires, J. D., 2005. Numerical Analysis 8th

800

edition. Thomson Brooks/Cole, Belmont, CA, USA, pp.

801

285, 343.

802

Chamberlain, J. W., 1960. Interplanetary Gas. II. Expansion of a

803

model of the Solar Corona. *Astrophys. J* 131, pp. 47-56.

804

Chamberlain, J. W., 1961. Interplanetary Gas. III. Hydrodynamic

805

Model of the Corona. *Astrophys. J* 133, pp. 675-687.

806

Chamberlain, J. W., Hunten D., 1987. Theory of Planetary

807

Atmospheres. Academic Press, New York.

808

Chapman, S. and Cowling, T. G., 1970. The Mathematical Theory

809

of Non-uniform Gases 3rd edition. Cambridge University

810

Press, New York, Chapter 10.

811

Elliot, J. L., et al., 2007. Changes in Pluto's Atmosphere: 1988-

812

2006. *Astrophys. J.* 134, pp. 1-13.

813

Greaves, J. S., Helling, Ch., Friberg, P., 2011. Discovery of

814

carbon monoxide in the upper atmosphere of Pluto. *Mon.*

815

Not. R. Astron. Soc. 000, pp. 1-6.

816

Gruzinov, A., 2011. The rate of thermal atmospheric escape.

817

arXiv:1101.1103v1 [astro-ph.EP] 5 Jan 2011.

818

819 Hubbard, W. B., Yelle, R. V., and Lunine, J.I., 1990.

820 Nonisothermal Pluto Atmosphere Models. *Icarus* 84, pp. 1-

821 11.

822 Hunten D. M., 1973. The Escape of Light Gases from Planetary

823 Atmospheres. *J. Atmos. Sci.* 30, pp. 1481-1494.

824 Hunten, D. M. and Watson, A. J., 1982. Stability of Pluto's

825 Atmosphere. *Icarus* 51, pp. 665-667.

826 Jeans, J. H., 1916. *The Dynamical Theory of Gases: The Outer*

827 *Atmosphere*. Cambridge University Press, pp. 351- 363.

828 Johnson, R. E., 2010. Thermally Driven Atmospheric Escape.

829 *Astrophys. J* 716, pp. 1573-1578.

830 Krasnopolsky, V. A., 1999. Hydrodynamic flow of N₂ from Pluto.

831 *J. Geophys. Res.* 104, pp. 5955-5962.

832 Lammer, H. et al., 2009. Determining the mass loss limit for close-

833 in exoplanets: what can we learn from transit observations?

834 *A & A* 506, pp. 399 - 410.

835 Marconi, M.L., Dagum, L., Smyth W.H., 1996. Hybrid fluid/

836 kinetic approach to planetary atmospheres: An example of

837 an intermediate mass body. *Astrophys. J.* 469, pp. 393-401.

838 McNutt, R. L., 1989. Models of Pluto's Upper Atmosphere.

839 *Geophysical Research Letters* 16, pp. 1225-1228

840 Murray-Clay, R. A.; Chiang, E. I, Murray, N., 2009 Atmospheric
841 Escape from Hot Jupiters. *Astrophys. J.* pp. 693, pp. 23-42.
842 Öpik, E.J., 1963. Selective escape of gases. *Geophys. J. Roy.*
843 *Astron. Soc.* 7, pp. 490-509.
844 Parker, E. N., 1958. Dynamics of the Interplanetary Gas and
845 Magnetic Fields. *Astrophys. J.* 128, pp. 664-676.
846 Parker, E. N., 1964a. Dynamical Properties of Stellar Coronas and
847 Stellar Winds. I. Integration of the Momentum Equation.
848 *Am. Astron. Soc.* 139, pp. 72-92.
849 Parker, E. N., 1964b. Dynamical Properties of Stellar Coronas and
850 Stellar Winds. II. Integration of the Heat-Flow Equation.
851 *Am. Astron. Soc.* 139, 93-122.
852 Strobel, D. F., 2008a. N₂ escape Rates from Pluto's atmosphere.
853 *Icarus* 193, pp. 612-619.
854 Strobel, D. F., 2008b. Titan's Hydrodynamically escaping
855 atmosphere. *Icarus* 193, pp. 588-594.
856 Tian, F., 2009. Thermal escape from super Earth atmosphere in the
857 habitable zone of M stars. *Astrophys. J.* 703, pp. 905–909.
858 Tian, F. and Toon, O. B., 2005. Hydrodynamic escape of nitrogen
859 from Pluto. *J. Geophys. Res.* L18201-L18205.
860 Trafton, L., 1980. Does Pluto have a Substantial Atmosphere?
861 *Icarus* 44, pp. 53-61.

862 Tucker, O. J., Erwin, J. T., Volkov, A. N., Cassidy, T. A., Johnson,
863 R. E., 2011. Escape from Pluto;s atmosphere: Fluid/DSMC
864 hybrid simulation. Proc. 27th International Symposium on
865 Rarefied Gas Dynamics, Pacific Grove, USA, 2010, AIP
866 Conf. Proc. 1333, pp. 1145-1150.

867 Tucker, O. J. and Johnson, R. E., 2009. Thermally driven
868 atmospheric escape: Monte Carlo simulations for Titan's
869 atmosphere. Planet Space Sci. 57, pp. 1889-1894.

870 Volkov, A. N., Johnson, R. E., Tucker, O. J. and Erwin, J. T.
871 2011a. Thermally-driven atmospheric escape: Transition
872 from hydrodynamic to Jeans escape. Astrophys. J. 729, pp.
873 L24.

874 Volkov, A. N., Tucker, O. J., Erwin, J. T. and Johnson, R. E.,
875 2011b. Kinetic Simulations of Thermal escape from a
876 single component atmosphere. Phys. Fluids 23, pp. 066601.

877 Watson, A. J. Donahue, T. M. and Walker J. C. G., 1981. The
878 Dynamics of a Rapidly Escaping Atmosphere: Applications
879 to the Evolution of Earth and Venus. Icarus 48, pp. 150-
880 166.

881 Yelle, R. V., 2004. Aeronomy of extra-solar giant planets at small
882 orbital distances. Icarus 170, pp. 167-179.

883 Young, E. F. et al., 2008. Vertical Structure in Pluto's Atmosphere
884 from the 2006 June 12 Stellar Occultation. *Astrophys. J.*
885 136, pp. 1757-1769.